

Vortex pinning by Ni point defects in $\text{Bi}_2\text{Sr}_2\text{Ca}(\text{Cu}_{1-x}\text{Ni}_x)_2\text{O}_{8+\delta}$ single crystals

R. Noetzel and K. Westerholt

Ruhr-Universität Bochum, Institut für Experimentalphysik IV, D-44780 Bochum, Germany

(Received 8 June 1998)

We study the vortex pinning of $\text{Bi}_2\text{Sr}_2\text{CaCu}_2\text{O}_{8+\delta}$ (Bi2212) single crystals doped with up to 2 at. % of Ni atoms on the Cu position using measurements of the dynamic magnetic relaxation. We find that below an optimum Ni-doping level of about 1 at. % the thermal activation energy for vortex creep and the critical current density definitely increase with the Ni concentration. This proves that Ni point defects contribute to the pinning forces, as expected within the theory of weak collective pinning. At higher Ni concentrations we observe a strong decrease of the activation energy, probably caused by an overlap of the vortex potentials from neighboring Ni sites. The dynamic behavior of the vortex system at low temperatures and magnetic fields is dominated by elastic creep of single vortices whereas at higher temperatures and fields plastic creep of vortex dislocations becomes dominant. The phase with plastic creep grows in the (B, T) plane with increasing strength of the collective pinning forces. [S0163-1829(98)00146-5]

I. INTRODUCTION

The physics of vortices in type-II superconductors has been of central interest since the beginning of high- T_c research. The relevance of vortex physics for technical applications is obvious, but, it is also interesting as far as basic research is concerned, since a variety of new vortex phases with different dynamic properties have been predicted and observed experimentally.¹⁻⁴

The complexity of the vortex phase diagram in the (B, T) plane of high- T_c compounds is due to the layered structure with superconducting CuO_2 planes separated by nonsuperconducting blocks. This strong anisotropy leads to a modulation of the superconducting order parameter along the c axis. The flux lines in an external magnetic field parallel to the c axis of the crystal are a build up of pancakelike supercurrent loops.^{1,5} Depending on the anisotropy, the temperature, and the magnetic field the vortex lines may behave as rigid three-dimensional objects or as stacks of nearly independent two-dimensional objects.⁵

The second important feature that causes the complexity of vortex physics in high- T_c superconductors is the presence of a random pinning potential leading to disorder in the vortex system. The dynamic response of the vortices to an external driving force is determined by a competition between the interaction of the vortices with the pinning potential and the vortex-vortex interactions. Changing the external magnetic field or the temperature, the dominant interaction and the coupling strength of pancake vortices in neighboring CuO_2 layers can be varied and consequently many different phases or subphases may occur in the (B, T) plane. Ordered vortex lattices,⁶ vortex glasses with different sources of static disorder,⁷⁻⁹ vortex line liquids,¹⁰ and even pancake-vortex gas phases¹¹ have been discussed in the literature.

The discussion of the microscopic origin of the weak random pinning potential, existing in all high- T_c superconductors, even in pure, high-quality single crystals, is still somewhat controversial.^{1,12} It is usually assumed that point defects such as oxygen vacancies or interstitial atoms are the main source of this pinning potential.¹³⁻¹⁵ These point de-

fects act collectively on the vortices in the sense that many of them contribute to the pinning potential seen by a vortex line. This is the basis for the collective pinning theory, which is established as an adequate model for the description of pinning in pure high- T_c superconductors.^{16,17}

Principally the random weak pinning potential can be modified by introducing point defects intentionally and actually this is the idea of the present work, where we want to study the pinning properties of Ni atoms on the Cu position in $\text{Bi}_2\text{Sr}_2\text{CaCu}_2\text{O}_{8+\delta}$ single crystals. The change of the integrated pinning forces caused by these additional point defects is difficult to predict. On the one hand, it is expected that the pinning force and the critical current density should increase with the number of defects¹ but, on the other hand, a high defect density enhances the disorder of the vortex lattice and this might be detrimental for the pinning forces.

Experimentally, magnetic relaxation measurements have given information on the pinning properties in high- T_c superconductors.¹⁸ The analysis of magnetic relaxation data is usually based on the assumption that below the irreversibility line vortices move through the sample by thermal activation. The main parameter determining the magnetic relaxation of the system is the effective thermal activation energy for vortex motion $U(j_s, H_e, T)$. Following the theories for weak collective pinning^{1,16,17} or vortex glasses^{3,19} U depends on the induced current density j_s , the external magnetic field H_e , and the temperature T . In our analysis below we use the following parametrization for the activation energy:²⁰

$$U(j_s) = \frac{U_c}{\mu} \left[\left(\frac{j_c}{j_s} \right)^\mu - 1 \right]. \quad (1)$$

This formula, which has often been used for the analysis of magnetic relaxation data in the literature²⁰⁻²² is quite general, since it contains the classical Kim-Anderson model²³ for high current densities $j_s \rightarrow j_c$ and also the divergence of U in the low-current limit, as expected within collective pinning theory or vortex glass models. These theories predict a definite set of positive numbers for the dynamic exponent,

TABLE I. Data of the $\text{Bi}_2\text{Sr}_2\text{Ca}(\text{Cu}_{1-x}\text{Ni}_x)_2\text{O}_{8+\delta}$ crystals used for the present study. Columns 1,2, crystal numbers and Ni concentrations determined from microprobe analysis; columns 3,4, total crystal mass and the geometrical factor Ω (see main text); columns 5,6, the transition temperature (susceptibility onset) and the extrapolated residual resistivity; columns 7,8, parameters C and $U_c(T \rightarrow 0)$ derived by the use of Eq. (4).

Crystal	x_{Ni} (at.%)	m (mg)	Ω (A/Gcm ²)	T_c (K)	$\varrho_n(\mu\Omega \text{ cm})$	C	U_0 (K)
b5-12	pure	7.92	165	85.5	80	13.0	130±10
b5-13	pure	0.84	362	85.7	75	21.4	130±10
na-10	0.66	2.51	240	82.9	101	17.2	140±20
nb-20	0.87	6.69	169	81.2	118	26.7	180±15
nb-12	0.89	1.56	281	79.5	125	15.0	180±10
nc-11	1.71	2.68	250	74.2	180	23.5	100±10
nd-10	1.80	3.92	119	73.7	340	13.5	100±10

e.g., $\mu = \frac{1}{7}$ for single vortex pinning (SVP), $\mu = \frac{5}{2}$ for small-bundle pinning, and $\mu = \frac{7}{9}$ for large-bundle pinning. In vortex glasses $\mu = \frac{1}{2}$ is expected for a three-dimensional (3D) elastic manifold.¹

Equation (1) contains a logarithmic divergence as a special case for $\mu \rightarrow 0$ and formally also allows for negative values of the exponent μ . This is physically meaningful in the case of plastic motion of dislocations in a regular vortex lattice²⁴ with the corresponding exponent being $\mu = -\frac{1}{2}$. Recent publications on the vortex dynamics based on Eq. (1) revealed that for strongly anisotropic high- T_c superconductors such as $\text{Tl}_2\text{Ba}_2\text{CaCu}_2\text{O}_{8+\delta}$ plastic vortex dislocation creep is dominant in the magnetic phase diagram below the irreversibility line.²²

In the present paper we study the pinning properties of $\text{Bi}_2\text{Sr}_2\text{CaCu}_2\text{O}_{8+\delta}$ single crystals doped with different concentrations of Ni on the Cu site by using the method of dynamic relaxation. We are mainly interested in the evolution of the pinning properties and the dynamic behavior of the vortex system with increasing degree of Ni substitution. In a previous publication we have found that Ni doping shifts the irreversibility line of Bi2212 single crystals to higher magnetic fields for doping levels $x \leq 1$ at. %, whereas a further increase of the Ni concentration causes a strong decrease of the irreversibility fields.²⁵ However, the correlation between the position of the irreversibility line within the (B, T) plane and the pinning forces is not straightforward.^{26,27} Measurements of the effective activation energy in the flux creep regime below the irreversibility line should give more insight into the pinning properties.

This paper is organized as follows: After a short description of the samples and the experiments, we introduce the method of dynamical relaxation and present the relaxation measurements of Ni-doped Bi2212 single crystals. The final section gives the conclusions and a summary.

II. EXPERIMENT

A. Samples and experimental method

We used single crystals of the high- T_c system $\text{Bi}_2\text{Sr}_2\text{CaCu}_2\text{O}_{8+\delta}$ doped with up to 2 at. % Ni on the Cu position for the present investigation. In a detailed study we have shown that single crystals of Bi2212 with a homogeneous Ni distribution can be grown by a modified Bridgman-Stockbarger technique.^{28,29} For the magnetic relaxation mea-

surements seven crystals containing different Ni concentrations were selected. The parameters characterizing these crystals are summarized in Table I.

Prior to the experiments the samples were subjected to an oxygen homogenization treatment by annealing in an atmosphere of 90% Ar and 10% O₂ at 780 °C for three days. The Ni-concentrations given in Table I were determined by quantitative x-ray wavelength dispersive microprobe analysis. For a first characterization of the superconducting properties we measured the ac susceptibility and the resistivity of the crystals. The real part of the ac susceptibility for five crystals from Table I measured with an ac amplitude of 0.1 Oe at 77 Hz is shown in Fig. 1. The superconducting transition shifts continuously towards lower temperatures with a slope of about -6 K/at. %. Only for the highest doping level $x = 1.8$ at. % Ni a slight broadening of the transition is observed. The residual resistivity extrapolated from the linear $\varrho(T)$ curve above T_c increases by about 150 $\mu\Omega \text{ cm}$ per at. % Ni substitution²⁹ (see Table I).

For applying the method of dynamic relaxation we measured magnetic hysteresis loops by a vibrating sample magnetometer (Lake Shore Model 7300) at different magnetic-field sweep rates $S \equiv dH_e/dt$ ranging from 5 Oe/s to 300 Oe/s. The magnetic field was always orientated parallel to the c axis of the single crystals, it was generated by a superconducting solenoid. The constant sweep velocity was established by a motor-driven high-precision potentiometer and controlled by a commercial Hall probe. During a field sweep the temperature of the sample was stabilized to better than 50 mK.

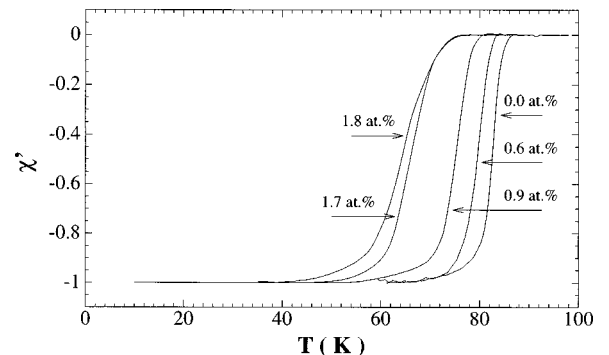


FIG. 1. Real part of the ac susceptibility measured at $f = 77$ Hz and $h_{ac} = 0.1$ Oe for Ni-doped Bi2212 single crystals from Table I.

B. Dynamic relaxation method

The dynamic relaxation method was pioneered, to the best of our knowledge, by Pust³⁰ and further developed by other groups.^{31–34} Recently it was applied to various high- T_c compounds.^{21,22} The method has often been shown to be equivalent to conventional relaxation measurements and can be used to extend the time window down to short relaxation times in the ms range,^{32,33} which can hardly be reached by conventional methods.¹⁸ The short relaxation times accessible in dynamic relaxation experiments are favorable in the case of high- T_c superconductors since the relaxation in these compounds can be very rapid.²⁰

The flux creep equation can be written as³¹

$$-\frac{dM}{dt} = \chi_0 \frac{dH_e}{dt} - \Delta v_0 H_e \exp\left(\frac{-U(j_s, H_e, T)}{k_B T}\right) \quad (2)$$

with the differential susceptibility χ_0 and the geometrical factor Δ only depending on the size and shape of the crystal,³¹ v_0 is the vortex hopping velocity. During a typical field sweep $\chi_0 dH_e/dt \gg dM/dt \propto dj_s/dt$ is always fulfilled in our experiment and thus the left-hand side in the flux creep equation (2) can be neglected. With the definition of the dynamic relaxation rate Q one can write

$$Q \equiv \frac{d \ln j_s}{d \ln S} = -\frac{k_B T}{j_s} \left(\frac{dU_j}{dj_s}\right)^{-1}. \quad (3)$$

The index j denotes the dependence of the effective activation energy on the normalized current density $j = j_s/j_c$. For the determination of U_j two experimental quantities are needed, the dynamic relaxation rate Q and the induced superconducting current density j_s , both parameters have to be determined at the same field sweep rate S_0 .

For the evaluation of the current dependent activation energy U_j in Eq. (3) we use the scheme recently worked out for high- T_c superconductors by Schnack and Griessen³⁵ starting with the current dependence of the activation energy $U(j)$ as given by Eq. (1). With Eq. (3) then follows

$$\frac{T}{Q(T, H_e)} = \frac{U_c(T, H_e)}{k_B} + \mu(T, H_e) C T. \quad (4)$$

The parameter $C \equiv \ln(\Delta v_0 H_e / \chi_0 S)$ contains all factors depending on the geometry. One can use the experimental data for the determination of C since for sufficiently low derivatives dj_c/dT for $T \rightarrow 0$ one can extrapolate (after quantum tunneling corrections) (Refs. 21,35):

$$C = \lim_{T \rightarrow 0} -\frac{1}{Q} \frac{d \ln j_s}{d \ln T}. \quad (5)$$

From Eq. (4) one can see that in a $(T/Q$ vs $T)$ plot a straight line is expected if $\mu(T)$ is a constant, thus allowing a direct determination of U_c and μ . It has been shown that these parameters can be derived by this method for many high- T_c systems.^{21,22,35}

III. RESULTS AND DISCUSSION

In Fig. 2 we show hysteresis loops measured at five dif-

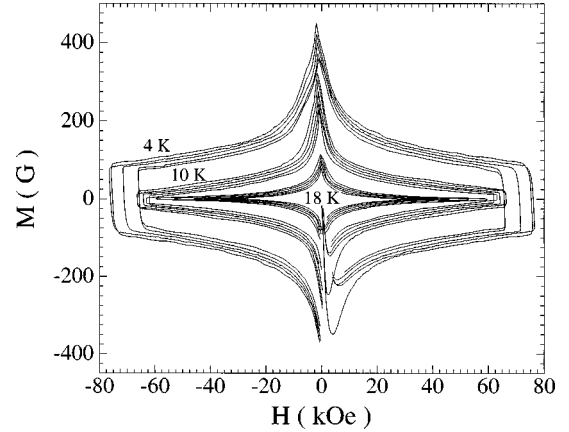


FIG. 2. Magnetic hysteresis loops of a Bi2212 single crystal doped with 0.9 at. % Ni (nb-12 from Table I). The magnetization curves were measured at 4 K, 10 K, and 18 K and field sweep rates $S = 5, 15, 45, 150, 300$ Oe/s (from the outer to the inner of the curves).

ferent field sweep rates from $S = 5$ Oe/s (inner curve) to $S = 300$ Oe/s (outer curve) for the sample nb-12, doped with 0.9 at. % Ni. For the sweep rate $S_0 = 45$ Oe/s (in the middle of the five curves) we calculated the induced current density $j_s = \Omega \Delta M$. The geometrical factor Ω was estimated for each crystal separately on the basis of the Bean model, considering a constant field gradient within the sample.³⁶ The Ω -values of all crystals are given in Table I. The current densities as a function of temperature derived from the hysteresis loops are shown in the upper panel of Fig. 3. For fields lower than $H_e = 5$ kOe the calculation of $j_s(T)$ was not done, because it cannot be assumed that the flux-profile is of the Bean type. Below the full-penetration field H^* interactions of the vortices with the shielding currents in the sample surface are not negligible and the flux profile may be dominated by the crystal geometry.^{27,37}

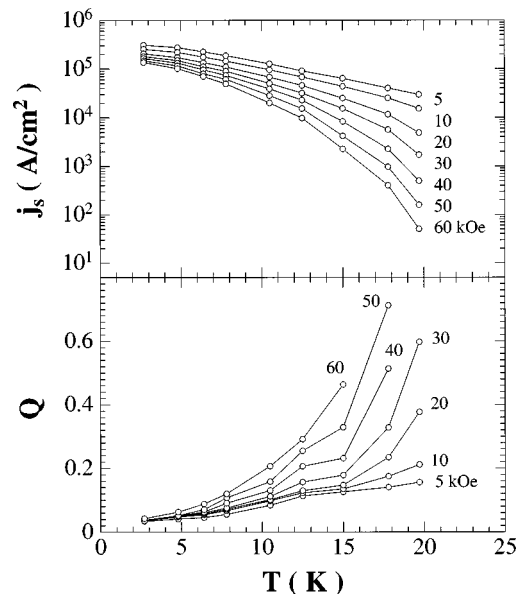


FIG. 3. Induced superconducting current density $j_s(T)$ (upper panel) and the normalized dynamic relaxation rate $Q(T)$ (lower panel) of the Bi2212 crystal with 0.9 at. % Ni derived for the sweep rate $S_0 = 45$ Oe/s and magnetic fields from 5 kOe to 60 kOe.

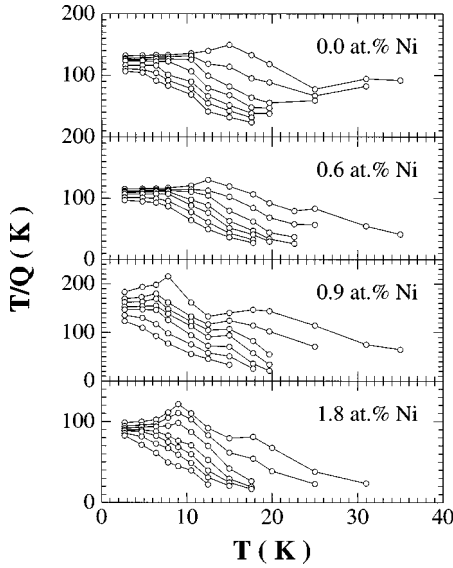


FIG. 4. $(T/Q$ vs T)-plot for four crystals from Table I. The external magnetic fields are $H_e = 5, 10, 20, 30, 40, 50$, and 60 kOe from the top curve to the bottom curve.

In the lower panel of Fig. 3 the logarithmic relaxation rate $Q = d \ln \Delta M / d \ln S$, defined as the mean slope of the irreversible magnetization at $S_0 = 45$ Oe/s, is plotted. Whereas the dynamic relaxation rate Q increases rapidly with the magnetic field and the temperature, the current density j_s decreases strongly. For $H_e = 50$ kOe for example, the dynamic relaxation rate reaches $Q = 1$ at $T \approx 20$ K. A relaxation rate of this order of magnitude indicates the vicinity of the irreversibility line in the magnetic phase diagram.²²

For an evaluation of the microscopic parameters U_c and μ following the scheme based on Eq. (4) we must replot the $Q(T)$ data in a $(T/Q$ vs T) diagram as outlined above. Since only thermal activated vortex hopping is considered in Eqs. (2)–(4), we have to subtract the quantum tunneling relaxation rate Q_0 , which can contribute considerably to the relaxation rate in the low-temperature range.^{21,38} We determined the rate Q_0 by extrapolating the $Q(T)$ curves linearly towards $T = 0$. As shown in a recent detailed study on quantum tunneling relaxation, Q is linear in temperature down to the mK regime for Bi2212 single crystals.³⁸ The fact that the $Q(T)$ curves in Fig. 3 approach one universal curve for $T \rightarrow 0$ shows that the dependence of Q_0 on the magnetic field is only weak. The T/Q -curves determined after subtraction of the quantum tunneling contribution are plotted for four Ni concentrations and different external fields in Fig. 4.

The prefactor $U_c(T)$ in Eq. (4) is expected to vary weakly for low temperatures, thus one would expect the T/Q plots to be straight lines for constant μ values. In contrast, all curves shown in Fig. 4 exhibit a definite nonlinear structure indicating that the dynamic exponent changes with the temperature and the magnetic field. Nevertheless, one can evaluate $U_c(H_e)$ from the low-temperature parts of the T/Q plots by linear extrapolation towards $T = 0$ with an accuracy of about 10–20 K. In the pinning models U_c plays the role of the energy scale for thermally activated vortex hopping.^{1,2} The resulting $U_c(T = 0)$ for the T/Q plots in Fig. 4 are presented as a function of the external magnetic field H_e in Fig. 5. For all crystals we derive an activation energy of the order 100

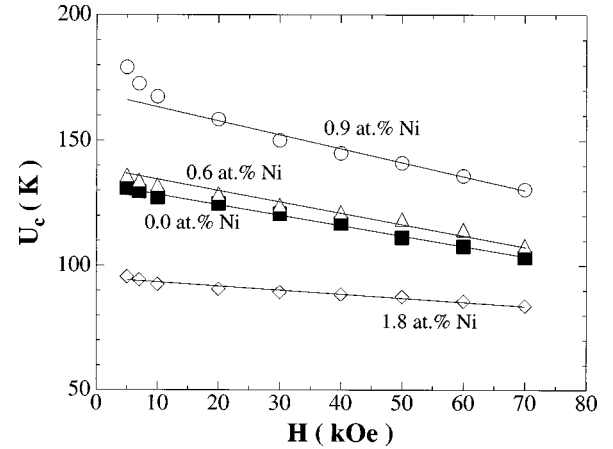


FIG. 5. The effective thermal activation energy $U_c(H)$ extrapolated for $T \rightarrow 0$ for the four crystals from Fig. 4.

K, very similar to the value obtained for Tl2212 films²² but significantly smaller than $U_c \approx 300$ K, obtained for $\text{YBa}_2\text{Cu}_3\text{O}_{7-y}$ -films.²¹ The numerical values of U_c for the Ni-doped Bi2212 crystals for $H_e \rightarrow 0$ and $T \rightarrow 0$ are also listed in Table I.

Consistent with previous results in the literature we find for all crystals a slight decrease of U_c with increasing magnetic field.²² Within the collective pinning model a strong increase of $U_c(H)$ is expected for small- or large-bundle pinning, whereas $U_c(H)$ should remain constant in the case of single-vortex pinning.¹ The slight decrease of the activation energy with the external field observed in Fig. 5 may be a consequence of the variation in the depths of the random potential valleys seen by a single vortex. With increasing number of vortices in the sample their adjustment to the effective pinning potential gets worse. The measured effective U_c , representing the average potential, will be slightly reduced then. In any case, only single-vortex pinning allows for the weak field dependence of $U_c(H)$ which is observed experimentally. If plastic dislocation creep is dominant, one expects^{22,24} $U_c \propto U_{pl} \propto H_e^{-(1/2)}$, but the experimental data in Fig. 5 with a linear slope of about -0.3 K/kOe do not follow this relation. Therefore we conclude that the flux movement at low temperatures is dominated by elastic creep of single pinned vortices.

Figure 5 also gives the dependence of U_c on the Ni concentration. It is obvious that the substitution of 0.9 at. % Ni gives a strong enhancement of U_c compared to pure Bi2212. This effect is well reproducible and can be measured in all crystals with similar doping levels. It clearly indicates that Ni atoms act as pinning centers on the Cu site of Bi2212. Figure 5 also reveals that the activation energy $U_c(H_e)$ decreases again for higher Ni-doping levels, i.e., it shows that Ni concentrations $x > 1$ at. % are detrimental for the pinning forces. In order to elaborate on this characteristic more systematically, we have plotted U_c at $H_e = 5$ kOe for the complete set of Ni-doped Bi2212 samples from Table I in Fig. 6(a). One sees that additional point defect pinning becomes perceptible at a Ni substitution of about $x = 0.5$ at. % and grows towards a doping level of $x \approx 1$ at. %, where U_c is enhanced by a factor of about 1.5 compared to the value for pure Bi2212 single crystals. For higher Ni concentrations the activation energy decreases to $U_c \approx 100$ K at $x = 1.8$ at. %, and

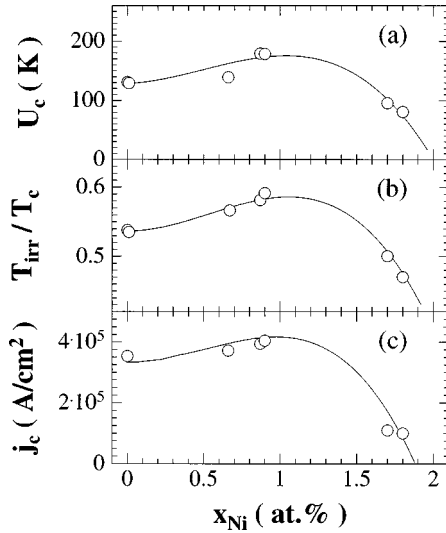


FIG. 6. Thermal activation energy $U_c(x)$ (a), reduced irreversibility temperature $t_{irr}(x) = T_{irr}(x)/T_c(x)$ (b) and critical current density $j_c(x)$ (c) at an applied field of $H = 5$ kOe as a function of the Ni concentration for all crystals from Table I. The drawn lines are guides to the eye.

which is definitely lower than U_c derived for pure Bi2212.

A similar nonmonotonous concentration dependence observed for $U_c(x)$ is also present in the shift of the irreversibility line.²⁵ For a direct comparison we have plotted the reduced irreversibility temperatures $t_{irr} = T_{irr}/T_c$ derived from ac-susceptibility measurements for the same external field $H_e = 5$ kOe in Fig. 6(b). The strong correlation between $U_c(x)$ and $t_{irr}(x)$ emphasizes that the interpretation of the irreversibility line for $H > 5$ kOe as a depinning line in Bi2212 is reasonable. In Fig. 6(c) we also plotted the critical current densities $j_c(x)$, details of the j_c determination will be given below. The main result here is that within the experimental error bars $j_c(x)$ has a concentration dependence identical to $U_c(x)$. Again this is consistent with the theory of weak collective pinning in high- T_c superconductors.¹

It is plausible that a certain density of Ni-point defects on the Cu position in a high- T_c superconductor can increase the effective pinning forces, since we expect that the superconducting pair density at the Ni position is lowered (δT_c pinning). However, the question arises, why a further increase of the Ni-point defect density beyond the critical doping level $x \geq 1$ at. % leads to the observed strong suppression of $U_c(x)$ and $j_c(x)$ (Fig. 6). A possible explanation for this nonmonotonous concentration dependence is suggested from numerical simulations of pinning potentials due to randomly distributed point defects.³⁹ The deformation of the vortex potential created by a real point defect like a Ni ion on the Cu position has a certain spatial extension. In the numerical simulation one finds a strong suppression of j_c and U_c setting in when the individual point defect potentials begin to overlap. Depending on the detailed shape of the local pinning potential, one therefore gets an optimum point defect density. In our experiments we estimate $x_{opt.} \sim 1$ at. % for Ni doping in Bi2212, this corresponds to an average Ni-ion distance of about 35 Å. However, besides the Ni atoms introduced intentionally there is a certain density of intrinsic point defects as oxygen vacancies or other structural defects. An-

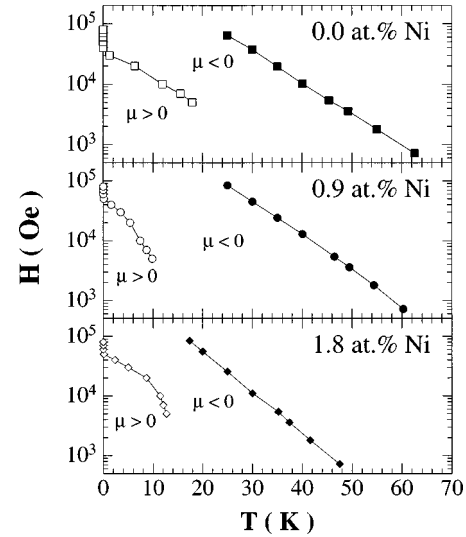


FIG. 7. Magnetic phase diagrams for a pure Bi2212 crystal, an optimally Ni-doped crystal (0.9 at. %) and a Ni-overdoped crystal (1.8 at. %). The empty symbols denote the transition line from elastic to plastic vortex creep ($\mu = 0$ line). The filled symbols give the irreversibility line as determined from ac-susceptibility measurements in Ref. 25.

other complication that prohibits a quantitative analysis of the microscopic pinning parameters is the fact that the distribution of Ni atoms in the crystals may not be uncorrelated. It is possible that some tendency towards clustering of Ni atoms exists at higher concentrations.

The second important parameter that can be derived from the plots in Fig. 4 is the exponent μ , characterizing the dependence of the activation barrier on the normalized current density j_s/j_c . For the crystals studied in the present work the values for the parameter C determined following equation (5) are given in Table I. Note that the dependence of C on both the external field H_e and the sweep rate S is weak within the experimental conditions of the present investigation, therefore we regard C in the analysis of our data as constant. From μC , determining the slope of the $T/Q(T)$ plot [see Eq. (4)], the dynamic exponent can be derived. A small positive exponent $\mu = 0.1 \dots 0.2$, as predicted in the collective pinning theory or in vortex glass models, is found for fields $H_e < 40$ kOe at low temperatures. Within the experimental error bars this value coincides with the exponent for single-vortex pinning (SVP) $\mu = \frac{1}{7}$. This result shows that the vortices in Bi2212 at low fields and temperatures are well described by the SVP theory.

Above about 10 K the slope in the $T/Q(T)$ plots becomes negative. Within a narrow temperature interval the dynamic exponent drops to a value $\mu \approx -0.3 \dots -0.4$. This effect was also reported recently for other high- T_c superconductors.^{22,24} As discussed above, a negative exponent μ indicates a phase with dislocation-mediated plastic vortex creep. The μ values obtained experimentally in this regime are close to the theoretical exponent $\mu = -\frac{1}{2}$, which is expected within a model based on diffusion of dislocations in atomic solids.²⁴ For $H_e \geq 40$ kOe the phase with plastic creep has displaced the SVP phase completely and even at very low temperatures μ remains negative.

To sum up the results obtained from the calculation of μ ,

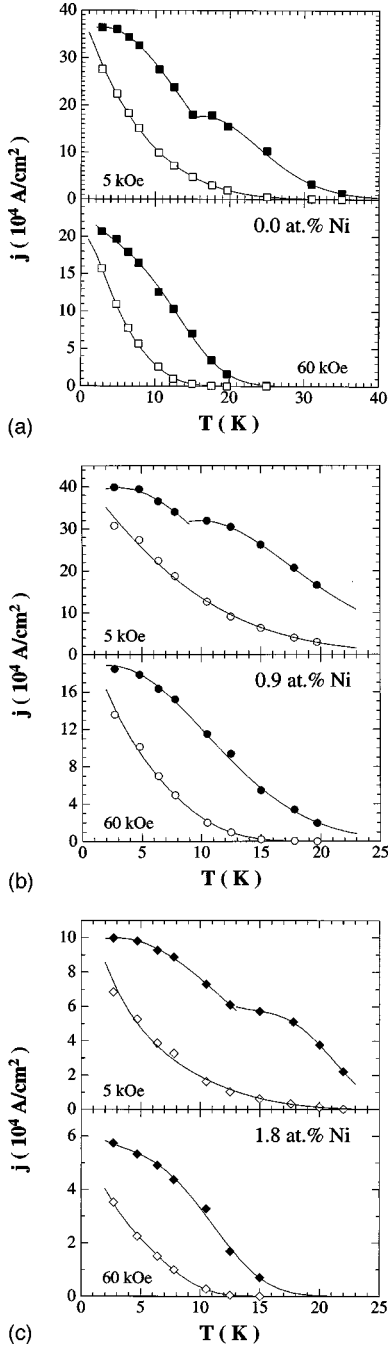


FIG. 8. Measured superconducting current density $j_s(T)$ at $S_0 = 45$ Oe/s (open symbols) and calculated critical current densities $j_c(T)$ (filled symbols). The current densities are plotted for a pure Bi2212 crystal (a) and crystals doped with 0.9 at. % Ni (b) and 1.8 at. % Ni (c). The external magnetic fields are $H = 5$ kOe and $H = 60$ kOe. The drawn lines represent fits with the empirical relation $j = j_0 \exp P_3(T)$ (see main text).

we have plotted the dynamic phase diagrams for pure, optimally Ni-doped and Ni-overdoped Bi2212 crystals in Fig. 7. We can distinguish three regimes within the (H, T) plane. At low temperatures and magnetic fields there is the elastic regime, where the collective pinning of single vortices determines the dynamic behavior, followed by the plastic phase, characterized by a dynamic exponent of the order $\mu \approx -\frac{1}{2}$. For the definition of the transition line (open symbols) we have chosen the intersection with $\mu(T) = 0$. The third vortex

phase above the irreversibility line $H_{irr}(T)$ (filled symbols) is interpreted as the vortex liquid. $H_{irr}(T)$ presented in Fig. 7 was derived from the ac-susceptibility loss peak measured at $h_{ac} = 0.1$ Oe and $f = 77$ Hz. The influence of the Ni-point defect concentration on the vortex dynamics becomes obvious by comparing the three diagrams in Fig. 7. $H_{irr}(T)$ for $H_e \geq 5$ kOe is largest at the optimum Ni concentration $x = 0.9$ at. % and decreases strongly at $x = 1.8$ at. %. Interestingly, the plastic-elastic transition temperatures shift in the opposite direction, i.e., the transition temperatures are lowest at the optimum degree of Ni substitution. Thus the optimum doping leads to a strong broadening of the plastic regime within the vortex phase diagram of Bi2212.

We finally calculate the critical current density j_c from the above results. By combining Eqs. (1) and (2) one gets the relation

$$j_c = j_s \left(\mu C \frac{k_B T}{U_c} + 1 \right)^{-\mu}. \quad (6)$$

In Figs. 8(a)–8(c) the resulting critical current densities (filled symbols) for three characteristic Ni concentrations are presented and compared to the measured current densities $j_s(T)$ (open symbols). One should note the large differences between the current densities $j_s(T)$ and $j_c(T)$. At $T = 20$ K the critical current density j_c is about a factor of 50 larger than j_s , even for $T \approx 2$ K the ratio is of the order 1.5. This means that the flux profiles, even in dynamic relaxation measurements using relatively high field sweep rates, are usually far away from the critical state. The decay of $j_c(T)$ in Fig. 8 can empirically be fitted by $j_c(T) \approx j_0 \exp P_3(T)$ with $P_3(T)$ being a polynomial of the third order. The exponential temperature dependence of the critical current density $j_c(T)$ is due to thermal fluctuations of vortices within the potential valleys and has been predicted theoretically for regions in the vicinity of the irreversibility line $H_{irr}(T)$.⁴⁰

It is remarkable that the transition from elastic to plastic vortex creep in phase diagrams in Fig. 7 can clearly be identified as a shoulder in the $j_c(T)$ curves in Fig. 8. The temperatures of this anomaly shown in the upper panels of Figs. 8(a)–8(c) coincide well with the corresponding transition temperatures plotted in Fig. 7. For $H_e = 60$ kOe the plastic-elastic transition is absent, consequently the corresponding $j_c(T)$ curves in the lower panels of Figs. 8(a)–8(c) are smooth.

IV. SUMMARY AND CONCLUSIONS

The analysis of the dynamic relaxation of Ni-doped Bi2212 single crystals based on a collective pinning model clearly demonstrates that up to a Ni concentration of about 1 at. % the pinning forces can be enhanced. At low temperatures the dynamical behavior can be described well by single-vortex pinning with an effective pinning energy $U_c(H_e = 0) \approx 130$ K for pure Bi2212 decreasing slightly with increasing magnetic field. The effective pinning energy can be enhanced up to $U_c \approx 180$ K for optimum doping at a Ni concentration of $x \approx 1$ at. %. Whereas experimentally the proof of point defect pinning by oxygen vacancies in $\text{YBa}_2\text{Cu}_3\text{O}_{7-y}$ and $\text{Bi}_2\text{Sr}_2\text{CaCuO}_{8+\delta}$ single crystals^{13,14} or by defects created by electron bombardment in Bi2212

samples⁴¹ was not very clear, our results strongly suggest the additional pinning by the Ni-point defects.

An increase of the density of Ni-point defects beyond the optimum concentration leads to a strong suppression of the parameters characterizing the strength of the pinning. In agreement with the results on the shift of the irreversibility line²⁵ one gets a nonmonotonous behavior of $U_c(x)$ and $j_c(x)$. A possible explanation for this effect is the compensation of the positive U_c enhancement from point defect pinning by an overlap of the individual defect potentials. This conclusion is supported by numerical computer simulations of point defect pinning.³⁹

Above the single-vortex pinning regime in the magnetic phase diagram the dynamic behavior of vortices in pure and Ni-doped Bi2212 can be explained by plastic motion of vortex dislocations. This seems to be typical for high- T_c superconductors and was recently also reported in YBaCuO crystals²⁴ and Tl2212 thin films.²² The transition from elastic to plastic creep is characterized by a change of the dynamic exponent μ within a narrow temperature interval from a positive to a negative value.

The crossover from elastic to plastic vortex dynamics is

also reflected in the temperature dependence of the critical current densities $j_c(T)$ where the changing sign of μ leads to a shoulder in the $j_c(T)$ curves. This shoulder reminds us of the second magnetization peak in $j_c(H)$ curves, observed in Bi2212 single crystals at low magnetic fields, which has also been discussed as a change of the vortex dynamics.^{24,42}

The elastic-plastic transition line in the (B, T) plane is correlated with the nonmonotonous concentration dependence of U_c and j_c but shifts in the opposite direction, i.e., an increasing U_c corresponds to a decrease of the transition temperature. One thus can conclude that a stronger pinning suppresses the elastic vortex phase within the magnetic phase diagram. A similar result was also obtained for electron irradiated Bi2212 single crystals.⁴¹ It is consistent with the idea that stronger pinning enhances the activation energy for elastic vortex motion but affects the plastic motion of dislocations to a much smaller extent.

ACKNOWLEDGMENT

The authors wish to thank the DFG for financial support of the present work.

-
- ¹G. Blatter, M. V. Feigelman, V. B. Geshkenbein, A. I. Larkin, and V. M. Vinokur, *Rev. Mod. Phys.* **66**, 1125 (1994).
- ²E. H. Brandt, *Physica C* **195**, 1 (1992).
- ³D. S. Fisher, M. P. A. Fisher, and D. A. Huse, *Phys. Rev. B* **43**, 130 (1991).
- ⁴L. F. Cohen and H. J. Jensen, *Rep. Prog. Phys.* **60**, 1447 (1997).
- ⁵J. Clem, *Phys. Rev. B* **43**, 7837 (1991).
- ⁶R. Cubitt, E. M. Forgan, G. Yang, S. L. Lee, D. McK. Paul, H. A. Mook, M. Yethiraj, P. H. Kes, T. W. Li, A. A. Menovsky, Z. Taranawski, and K. Mortensen, *Nature (London)* **365**, 407 (1993).
- ⁷H. Safar, P. L. Gammel, D. J. Bishop, D. B. Mitzi, and A. Kapitulnik, *Phys. Rev. Lett.* **68**, 2672 (1992).
- ⁸Quiang Li, H. J. Wiesmann, M. Suenaga, L. Motowidlow, and P. Haldar, *Phys. Rev. B* **50**, 4256 (1994).
- ⁹U. C. Tauber and D. Nelson, *Phys. Rev. B* **52**, 16 106 (1995).
- ¹⁰J. A. Fendrich, W. K. Kwok, J. Giapintzakis, C. J. van der Beek, V. M. Vinokur, S. Fleshler, U. Welp, H. K. Viswanathan, and G. W. Craptree, *Phys. Rev. Lett.* **74**, 1210 (1995).
- ¹¹C. D. Keener, M. L. Trawick, S. M. Ammirata, S. E. Hebboul, and J. C. Garland, *Phys. Rev. Lett.* **78**, 1118 (1997).
- ¹²R. Griessen, H. H. Wen, A. J. J. vanDalen, B. Dam, J. Rector, H. G. Schnack, S. Libbrecht, E. Osquiguil, and Y. Bruynseraede, *Phys. Rev. Lett.* **72**, 1910 (1994).
- ¹³C. J. van der Beek and P. H. Kes, *Phys. Rev. B* **43**, 13 032 (1991).
- ¹⁴M. Daeumling, J. M. Seuntjens, and D. C. Larbalestier, *Nature (London)* **346**, 332 (1990).
- ¹⁵H. Theuss, *Physica C* **208**, 155 (1993).
- ¹⁶V. M. Vinokur, M. V. Feigelman, V. B. Geshkenbein, and A. I. Larkin, *Phys. Rev. Lett.* **65**, 259 (1990).
- ¹⁷M. V. Feigelman, V. B. Geshkenbein, A. I. Larkin, and V. M. Vinokur, *Phys. Rev. Lett.* **63**, 2303 (1989).
- ¹⁸Y. Yeshurun, A. P. Malozemoff, and A. Shaulov, *Rev. Mod. Phys.* **68**, 911 (1996).
- ¹⁹M. P. A. Fisher, *Phys. Rev. Lett.* **62**, 1415 (1989).
- ²⁰M. Niderost, A. Suter, P. Visani, A. C. Mota, and G. Blatter, *Phys. Rev. B* **53**, 9286 (1996).
- ²¹A. J. J. van Dalen, R. Griessen, S. Libbrecht, Y. Bruynseraede, and E. Osquiguil, *Phys. Rev. B* **54**, 1366 (1996).
- ²²H. H. Wen, A. F. Th. Hoekstra, R. Griessen, S. L. Yan, L. Fang, and M. S. Si, *Phys. Rev. Lett.* **79**, 1559 (1997).
- ²³P. W. Anderson and Y. B. Kim, *Rev. Mod. Phys.* **36**, 39 (1964).
- ²⁴Y. Abulafia, A. Shaulov, Y. Wolfus, R. Prozorov, L. Burlachkov, Y. Yeshurun, D. Majer, E. Zeldov, H. Wuhl, V. B. Geshkenbein, and V. M. Vinokur, *Phys. Rev. Lett.* **77**, 1596 (1996).
- ²⁵R. Noetzel, B. vom Hedt, and K. Westerholt, *Physica C* **260**, 290 (1996).
- ²⁶M. Konczykowski, L. I. Burlachkov, Y. Yeshurun, and F. Holtzberg, *Phys. Rev. B* **43**, 13 707 (1991).
- ²⁷E. Zeldov, A. I. Larkin, V. B. Geshkenbein, M. Konczykowski, D. Majer, B. Khaykovich, V. M. Vinokur, and H. Shtrikman, *Phys. Rev. Lett.* **73**, 1428 (1994).
- ²⁸O. Bonfigt, H. Somnitz, K. Westerholt, and H. Bach, *J. Cryst. Growth* **128**, 725 (1993).
- ²⁹B. vom Hedt, W. Lisseck, K. Westerholt, and H. Bach, *Phys. Rev. B* **49**, 9898 (1994).
- ³⁰L. Pust, *Supercond. Sci. Technol.* **3**, 598 (1990).
- ³¹M. Jirsa, L. Pust, H. G. Schnack, and R. Griessen, *Physica C* **207**, 85 (1993).
- ³²H. G. Schnack, R. Griessen, J. G. Lensink, C. J. van der Beek, and P. H. Kes, *Physica C* **197**, 337 (1992).
- ³³Q. Wang and X. Yao, *Z. Phys. B* **101**, 151 (1996).
- ³⁴Z. M. Ji, R. X. Wu, G. D. Zhou, J. P. Zuo, J. Zhou, H. B. Wang, W. W. Xu, Q. H. Cheng, S. Z. Yang, P. H. Wu, J. F. Geng, and X. Jin, *J. Appl. Phys.* **82**, 6116 (1997).
- ³⁵H. G. Schnack and R. Griessen, *Physica C* **241**, 353 (1995).
- ³⁶H. P. Wiesinger, F. M. Sauerzopf, and H. W. Weber, *Physica C* **203**, 121 (1992).
- ³⁷R. I. Khasanov, Y. I. Talanov, W. Assmus, and G. B. Teitelbaum,

- Phys. Rev. B **54**, 13 339 (1996).
- ³⁸A. F. Th Hoekstra, A. M. Testa, G. Doornbos, J. C. Martinez, B. Dam, R. Griessen, B. I. Ivlev, M. Brinkmann, K. Westerholt, W. K. Kwok, and G. W. Cragtree, Phys. Rev. B (to be published).
- ³⁹J. Shumway and S. Satpathy, Phys. Rev. B **56**, 103 (1997).
- ⁴⁰M. V. Feigelman and V. M. Vinokur, Phys. Rev. B **41**, 8986 (1990).
- ⁴¹B. Khaykovich, M. Konczykowski, E. Zeldov, R. A. Doyle, D. Majer, P. H. Kes, and T. W. Li, Phys. Rev. B **56**, 517 (1997).
- ⁴²B. Khaykovich, E. Zeldov, D. Majer, T. W. Li, P. H. Kes, and M. Konczykowski, Phys. Rev. Lett. **76**, 2555 (1996).